Effect of Density Gradients in Confined Supersonic Shear Layers. Part II. 3-D Modes

by
O. Peroomian

The effect of basic flow density gradients on the supersonic wall modes were investigated in Part I of this analysis. In that investigation only the 2-D modes were studied. Tam and Hu investigated the 3-D modes in a confined vortex sheet and reported that the first 2-D Class A mode (A_{01}) had the highest growth rate compared to all other 2-D and 3-D modes present in the vortex sheet for that particular set of flow parameters. They also showed that this result also held true for finite thickness shear layers with $\delta_\omega < 0.125$. For free shear layers, Sandham and Reynolds showed that the 3-D K-H mode became the dominant mode for $M_c > 0.6$. Jackson and Grosch investigated the effect of crossflow and obliqueness on the slow and fast modes present in a $M_c > 1$ environment and showed that for certain combination of crossflow and wave angles the growth rates could be increased by up a factor of 2 with respect to the 2-D case. Two major differences between the confined and unconfined cases are the type of modes present in the two cases and the restriction on the spanwise wavenumber in the confined case. The modes present in a confined supersonic 2-D shear layer are of the acoustic type (wall modes) as opposed to the vorticity modes present in the free shear layer, and these wall modes have higher growth rates than the vorticity modes. Also, due to the side walls, the

confined shear layer only has discrete spanwise wavenumber solutions.

The case studied here is a confined shear layer shown in Part I. All solution procedures and basic flow profiles are the same as in Part I. The effect of density gradients on the 3-D modes present in the density ratios considered in Part I are investigated.

II. Flow Model and Governing Equations

As in Part I, the model which is studied here is a confined compressible shear layer formed by two gases with different velocities, densities and properties, but with the same constant pressure. Figure 1 shows the configuration used in this analysis. The subscript 1 is used for the quantities related to the high speed freestream and the subscript 2 for the quantities of the low speed freestream. The streamwise coordinate is x, the spanwise coordinate is z, and the cross-stream coordinate is y. The aspect ratio of the channel is taken to be 2 ($B^* = 2H^*$). For simplicity, free slip wall boundary conditions are assumed at the walls of the channel. It is also assumed that the flow is inviscid, non-conducting, and non-diffusive. For this situation the governing equations are the Euler equations for a two species system.

The equations are non-dimensionalized using the fast (upper) freestream

quantities, ρ_1^*, U_1^*, T_1^* and the height of the channel, H^*. Thermodynamic properties are also non-dimensionalized by the upper freestream thermodynamic properties, $c_{p_a}^*$ and R_a^*. Based on this non-dimensionalization, the density ratio $\frac{\rho_2^*}{\rho_1^*}$ and the velocity ratio $\frac{U_2^*}{U_1^*}$ are defined as ρ_2 and U_2, respectively. Once the equations are non-dimensionalized, they are linearized around a parallel basic flow $(\bar{\rho}(y), \bar{P}, \bar{U}(y), \bar{C}_a(y))$. These basic flow quantities can be found by solving the compressible boundary layer equations using a similarity variable for $Pr = Sc = Le \cong= 1$. This procedure was discussed in Part I.

Normal modes are assumed for these infinitesimal disturbances with the form:

$$q' = \hat{q}(y)\, exp[i(kx + \beta z - \omega t)] \tag{2.1}$$

where $\hat{q}$ is the eigenfunction, k and β are the streamwise and spanwise wave numbers and ω is the frequency. In general k, β and ω are complex. Once these normal modes are substituted into the equations of motion, a single O.D.E. can be found for the disturbance pressure eigenfunction:

$$D^2\hat{p} + \left\{\frac{2kD\bar{U}}{(\omega - k\bar{U})} - \frac{1}{\bar{\rho}}D\bar{\rho}\right\}D\hat{p} + \left\{\frac{\bar{\rho}\gamma_1 M_1^2}{\bar{\gamma}}(\omega - k\bar{U})^2 - k^2 - \beta^2\right\}\hat{p} = 0 \tag{2.2}$$

where

$$D = \frac{d}{dy}$$

$$\bar{\gamma} = \frac{c_{p_a}\bar{C}_a + c_{p_b}(1-\bar{C}_a)}{c_{v_a}\bar{C}_a + c_{v_b}(1-\bar{C}_a)}$$

and M_1 and γ_1 are, respectively, the Mach number and the ratio of specific heats of the high speed freestream.

The above equation is solved subject to the boundary conditions

$$D\hat{p} = 0 \qquad y = \pm\frac{1}{2} \tag{2.3a}$$

$$D\hat{p} = 0 \qquad z = \pm 1 \tag{2.3b}$$

which come from the y and z-momentum equations by setting the normal velocity at the walls to zero. It is the latter boundary condition that leads to a discrete spectrum of spanwise wavenumbers. Therefore the spanwise wavenumber becomes:

$$\beta = m\pi \tag{2.4}$$

for an aspect ratio of two, and the disturbance pressure takes the form:

$$p'(x,y,z,t) = \hat{p}(y)\, cos(m\pi z)\, exp[i(kx - \omega t)] \tag{2.5}$$

Outside the shear layer the vortex sheet solutions hold. They can be written as:

$$\hat{p}(y) = A\, cos[\lambda_1(1-y)] \qquad \delta < y \leq 1 \tag{2.6a}$$

$$\hat{p}(y) = B\, cos[\lambda_2(1+y)] \qquad -\delta > y \geq -1 \tag{2.6b}$$

where

$$\lambda_1 = [M_1^2(\omega - kU_1)^2 - k^2 - (m\pi)^2]^{\frac{1}{2}} \tag{2.7a}$$

$$\lambda_2 = [M_1^2\left(\frac{a_1^*}{a_2^*}\right)^2(\omega - kU_2)^2 - k^2 - (m\pi)^2]^{\frac{1}{2}} \tag{2.7b}$$

Following Mack, we define a 3-D wave number as:

$$\tilde{k} = (k^2 + (m\pi)^2)^{\frac{1}{2}} \tag{2.8}$$

one can also define a complex convective Mach number, $\bar{M}_c(y)$ as:

$$\bar{M}_c(y) = \sqrt{\frac{\bar{\rho}\gamma_1 M_1^2}{\bar{\gamma}\tilde{k}^2}(\omega - k\bar{U})^2} \tag{2.9}$$

therefore equation (2.2) can be written as:

$$D^2\hat{p} + \left\{\frac{2kD\bar{u}}{(\omega - k\bar{u})} - \frac{1}{\bar{\rho}}D\bar{\rho}\right\}D\hat{p} + \tilde{k}^2\left\{\bar{M}_c^2 - 1\right\}\hat{p} = 0 \tag{2.10}$$

This form of the O.D.E. for the disturbance pressure eigenfunction clearly shows the role of the parameter $\bar{M}_c$ and its significance in the type of solutions possible. Now, outside the shear layer for a neutral wave this convective Mach number is a constant real value, i.e. $(\bar{M}_{c1} = M_{c1}, \bar{M}_{c2} = M_{c2})$,

$$\bar{M}_{c1} = M_1\left(\frac{k\bar{U} - \omega}{\tilde{k}}\right) = M_1 cos\psi(1 - C_{phx}) \tag{2.11a}$$

and

$$\bar{M}_{c2} = M_1\left(\frac{a_1^*}{a_2^*}\right)cos\psi(U_2 - C_{phx}) \tag{2.11b}$$

where $C_{phx} = \frac{\omega}{k_r}$, and ψ is the wave angle. As shown for the 2-D case, when $M_{c2} > 1$ non-inflectional neutral solutions of the type $C_{phx} = 1$ are possible and when $M_{c1} > 1$ then non-inflectional neutral solutions of the type $C_{phx} = U_2$ are possible.

Based on the above definitions and the results obtained in Part I, the following cases are investigated:

$$Case I: \quad \rho_2 = 1.398 \quad m = 1$$

$$Case II: \quad \rho_2 = 1.398 \quad m = 3$$

$$Case III: \quad \rho_2 = 3.000 \quad m = 1$$

$$Case IV: \quad \rho_2 = 3.000 \quad m = 3$$

In all the cases, the fast stream gas is He and the slow stream gas is N_2. Also, the convective Mach number is 1.836, and the velocity ratio is 0.276.

Results and discussion

Case I

As shown in Part I, the basic flow profiles have three generalized inflection points giving rise to three separate types of modes. These modes are all

supersonic wall modes and the necessary condition for their existence is a trapped region of supersonic flow with respect to their phase speeds. In order to use this condition, the maximum convective Mach number in the channel, $|\bar{M}_c(y)|_{max}$, is plotted in the frequency and real wavenumber plane. Figure 2 shows the contours of this maximum convective Mach number. The dashed lines correspond to $|\bar{M}_c(y)|_{max} < 1$. Any modes which are present within the 'wedge' ($|\bar{M}_c(y)|_{max} = 1$) are subsonic with respect to both streams and therefore are not acoustic in nature. Figure 3 shows the real wavenumber vs. frequency of all the modes present when the spanwise wavenumber is fixed to $\beta = \pi$. The fine dashed line in the form of a wedge is the $|\bar{M}_c(y)|_{max} = 1$ line. Two modes originate in that wedge and are subsonic with respect to both streams until they exit the wedge. Figure 4 shows the phase speed of the modes present for this case. Several differences arise when we compare Figure 4 to Figure 6 in Part I. First, we now have a mode present in the limit as the frequency goes to zero. This mode is originally subsonic, and as it turns supersonic with respect to the fast stream it is very much like the combination of the first three 2-D Class B modes (upper portion of the phase speed curves in Figure 6 in Part I). This mode will be called the D_{11} mode. The first Class C mode C_{11} also starts from within the wedge described above, but its phase speed exits the wedge very quickly and only slightly changes the characteristics

of the mode. The rest of the Class A, B and C modes are all entirely acoustic modes and their phase speeds are similar to those in the 2-D case. One must note that the first two Class A and C modes are different in the sense that each has 'picked up' the other's phase speed curve. Figures 5a,b,c and d show the growth rate of the Class A,B,C and D modes respectively. The growth rate curve for the A_{12} mode has only one peak and its maximum growth rate is a few percent higher than than that of the 2-D mode. The growth rate curve for the A_{13} mode is almost identical to its 2-D counterpart despite the fact that the wave angle at the maximum growth rate of for this mode is about 30 degrees. Mode A_{11} has very small growth rates (as do modes B_{11}, B_{12}, B_{13}) and is not shown. Since the Class A and C modes have switched portions of their phase speed curves with one-another, one must also discuss the growth rates of the Class C modes with conjunction to the Class A modes. Instead of identifying the 2-D and 3-D counterparts of each growth rate peak, one can make a general statement that except for the A_{12}, in the region where the waves are 3-D, the growth rates are lower than those found for the 2-D case. In fact mode C_{11} has a growth rate which is about 25% lower than its 2-D counterpart. The growth rate curves of the class B modes are very much like the 2-D modes. The D_{11} mode present for this spanwise wave number has one subsonic growth rate peak and three supersonic peaks. The supersonic

portion of the phase speed curve for this mode is very much like the curve for the B_{01} mode for a density ratio of about 1.65 where the first three Class B modes have undergone a resonant interaction. In general, if one plots all the growth rates of the 2-D and 3-D modes ($\beta = \pi$), one will find that the C_{01} has the highest growth rate.

Case II

In this case, the density ratio is the same as above, but the spanwise wavenumber is now equal to 3π. Figure 6 shows the maximum convective Mach number contours. The wedge corresponding to the $|\bar{M}_c(y)|_{max} = 1$ contour is much larger than that in Case I. This implies that the region over which purely subsonic modes can exists is much greater. Figure 7 shows the real wavenumbers of the modes present when the spanwise wave number is set to 3π. Now both modes which start within the subsonic wedge have zero frequency limits and both will be labeled as Class D modes. Figure 8 shows the phase speed of the modes for this case. There are Class A,B and C modes with very small growth rates within this frequency region and are not shown. Figure 9a shows the growth rates for some of the Class A and B modes and Figure 9b for the Class D modes. Very much like Case I, it can be concluded that the 3-D modes have lower growth rates than the 2-D modes. Therefore

for the test case parameters the 2-D, the C_{01} mode has the highest growth rate. Tam and Hu also found similar results for their A_{01} mode.

Case III

This case corresponds to a density ratio of 3.0 for which the basic flow profiles only have one generalized inflection point. Thus, as shown in Part I, only Class A and B modes are present in the 2-D analysis. Figure 10 shows the real wavenumber for the modes present. Only one mode exist in the subsonic wedge and is present in the zero frequency limit. The phase speed vs. frequency is given in Figure 11 and Figures 12a and b show the growth rates of the Class A modes and the D_{11} mode respectively. The 3-D Class A modes for this case have smaller growth rates than their 2-D counterparts. Very much like Case I, the D_{11} modes' supersonic continuation is very similar to the B_{01} mode present for these parameters . Figure 13 shows the growth rates of both modes on the same graph. It can be seen from this figure that the maximum growth rate peak for the 3-D mode is slightly higher than the 2-D mode. More about the growth rate of this mode will be said in the next section.

Note that the Class B modes were not shown due to fact that they possess very small growth rates.

Case IV

The parameters for this case are the same as in Case III, however the spanwise wavenumber is increased to 3π. Figures 14 and 15 show the wavenumber and phase speed of the modes present. Again, like Case II the sonic wedge is much greater than for the smaller wavenumber (Case III). Figure 16 and 17 show the growth rates of the Class A and the D_{11} modes. The Class A modes have much lower growth rates than their 2-D counterparts. However, the D_{11} mode a higher growth rate (by 5 %) than the B_{01} mode. Also, the frequency for the maximum growth rate has shifted to the left. In order to investigate this effect further, the mode D_{11} for $\beta = 5\pi$ is calculated and its growth rate along with the D_{11} modes for $\beta = \pi$ and 3π and the B_{01} modes are plotted in Figure 18. It is clear from this figure that the rise in the growth rate due to the larger growth rates in the subsonic regions of these modes eventually stops and actually the growth rates start to decrease beyond a spanwise wavenumber of 5π.

Based on all the results shown for all the cases considered, one can conclude that 3-D effects are not that important in the sense that they don't give rise to much larger growth rates as is the case in free shear layer. However, they do give rise to modes which have almost the same phase speeds and growth

rates as the 2-D modes which can give rise to non-linear resonant interaction in the evolution of the full 3-D shear layer.

Fig 2

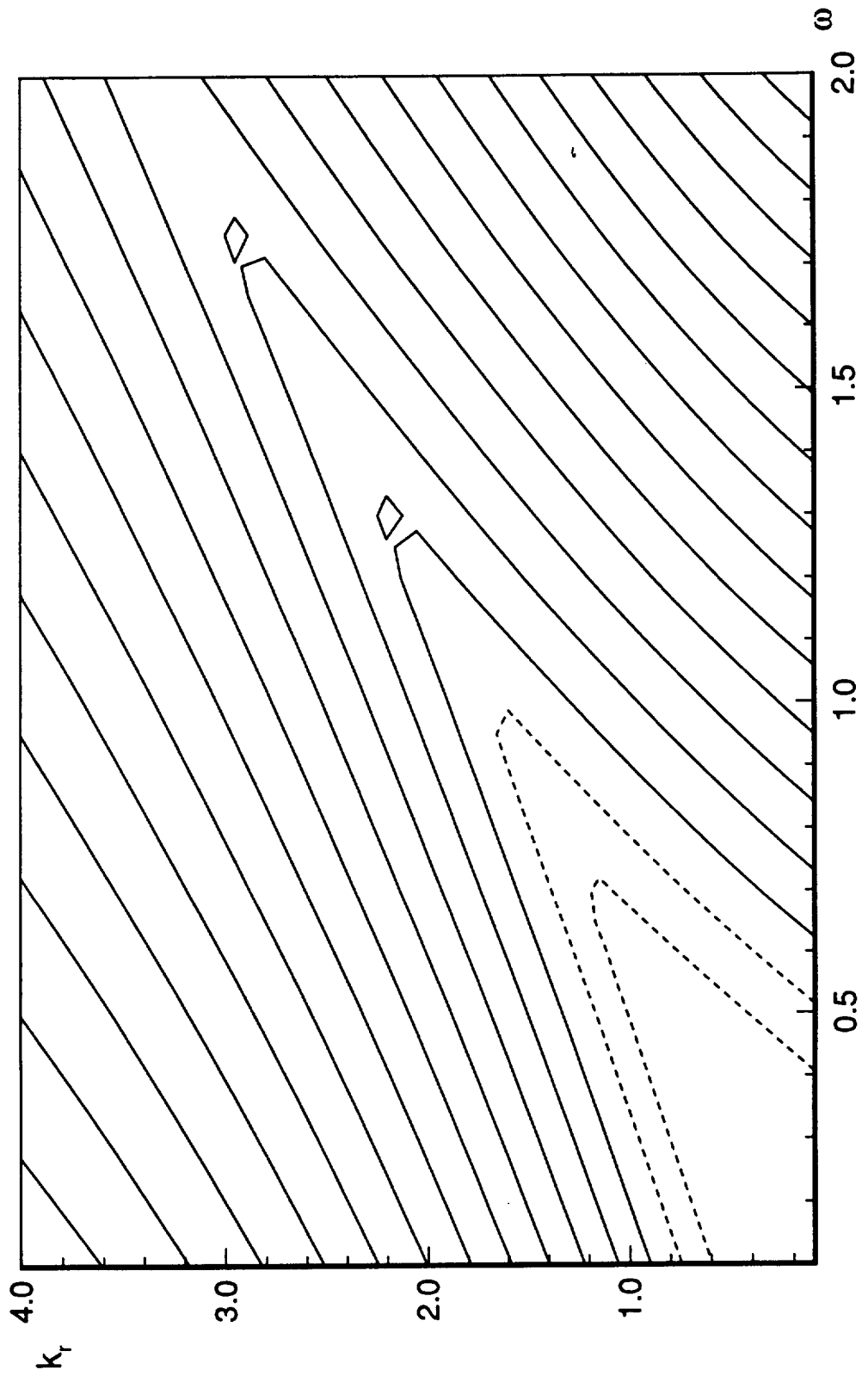

Streamwise Wavenumber vs. Frequency for All 3-D Modes

($B = 2H$, $\beta = 2m\pi/B$, $m=1$)

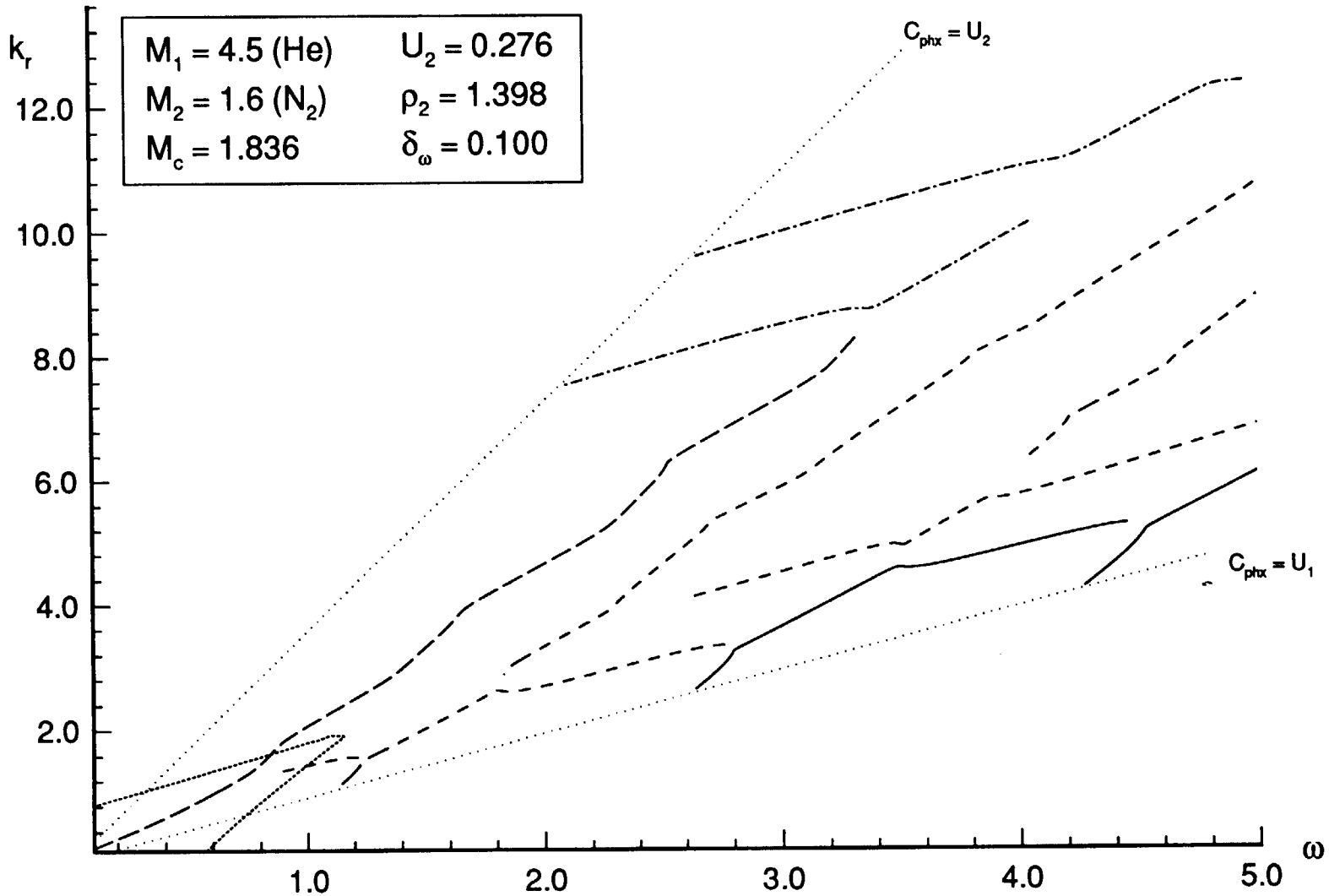

The triangular fine-dashed line is $|M_c(y)|_{max} = 1.0$

Phase Speed vs. Frequency for All 3-D Modes Based on the Boundary Layer Profiles

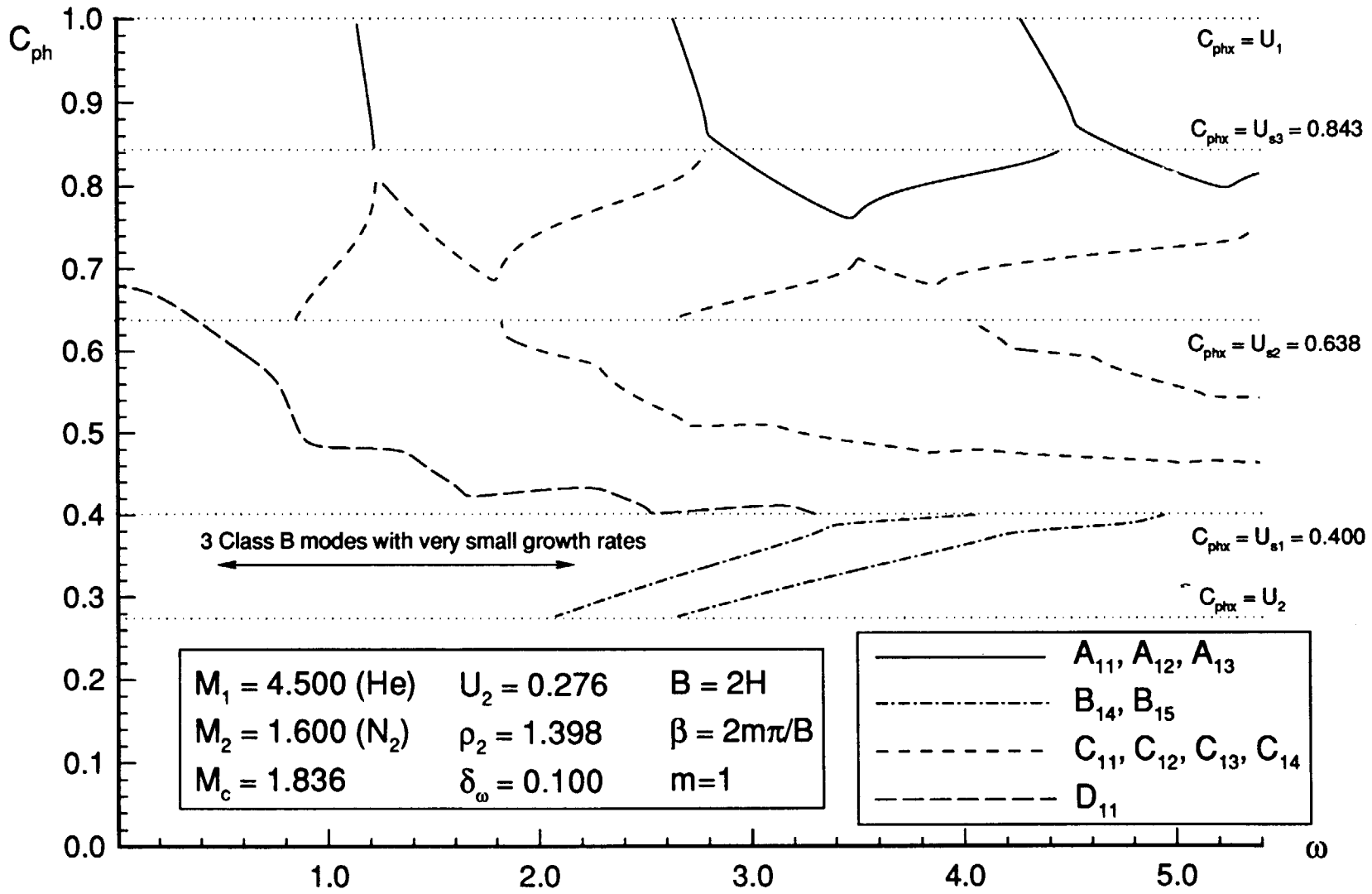

(5)a

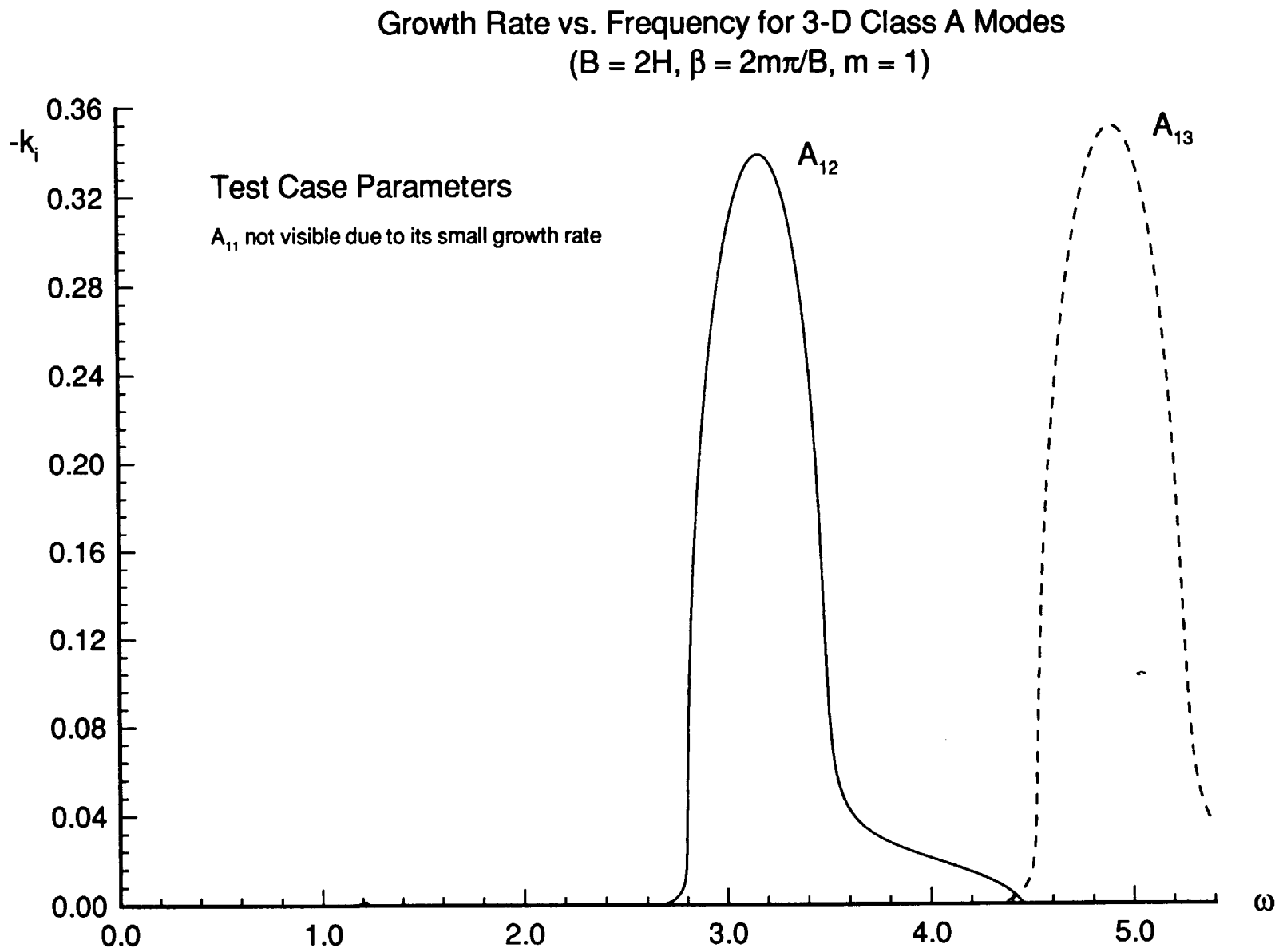
Growth Rate vs. Frequency for 3-D Class A Modes
(B = 2H, β = 2mπ/B, m = 1)
-k_i
0.36
0.32
0.28
0.24
0.20
0.16
0.12
0.08
0.04
0.00
0.0
1.0
2.0
3.0
4.0
5.0
ω
Test Case Parameters
A11 not visible due to its small growth rate
A12
A13

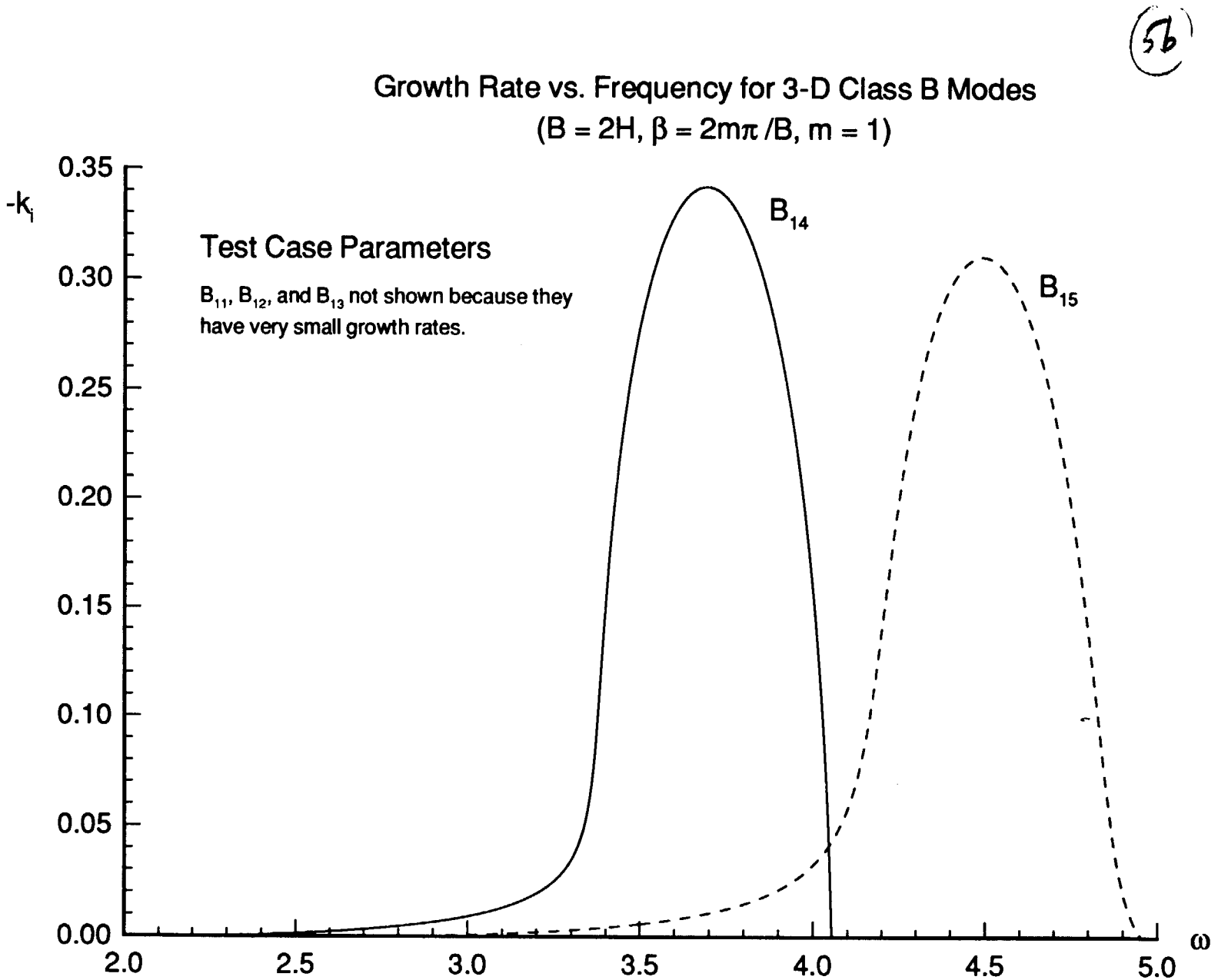
Growth Rate vs. Frequency for 3-D Class B Modes
(B = 2H, β = 2mπ /B, m = 1)
-k_i
0.35
0.30
0.25
0.20
0.15
0.10
0.05
0.00
2.0
2.5
3.0
3.5
4.0
4.5
5.0
ω
Test Case Parameters
B11, B12, and B13 not shown because they have very small growth rates.
B14
B15

Growth Rate vs. Frequency for 3-D Class C Modes
(B = 2H, β = 2mπ/B, m = 1)
Test Case Parameters

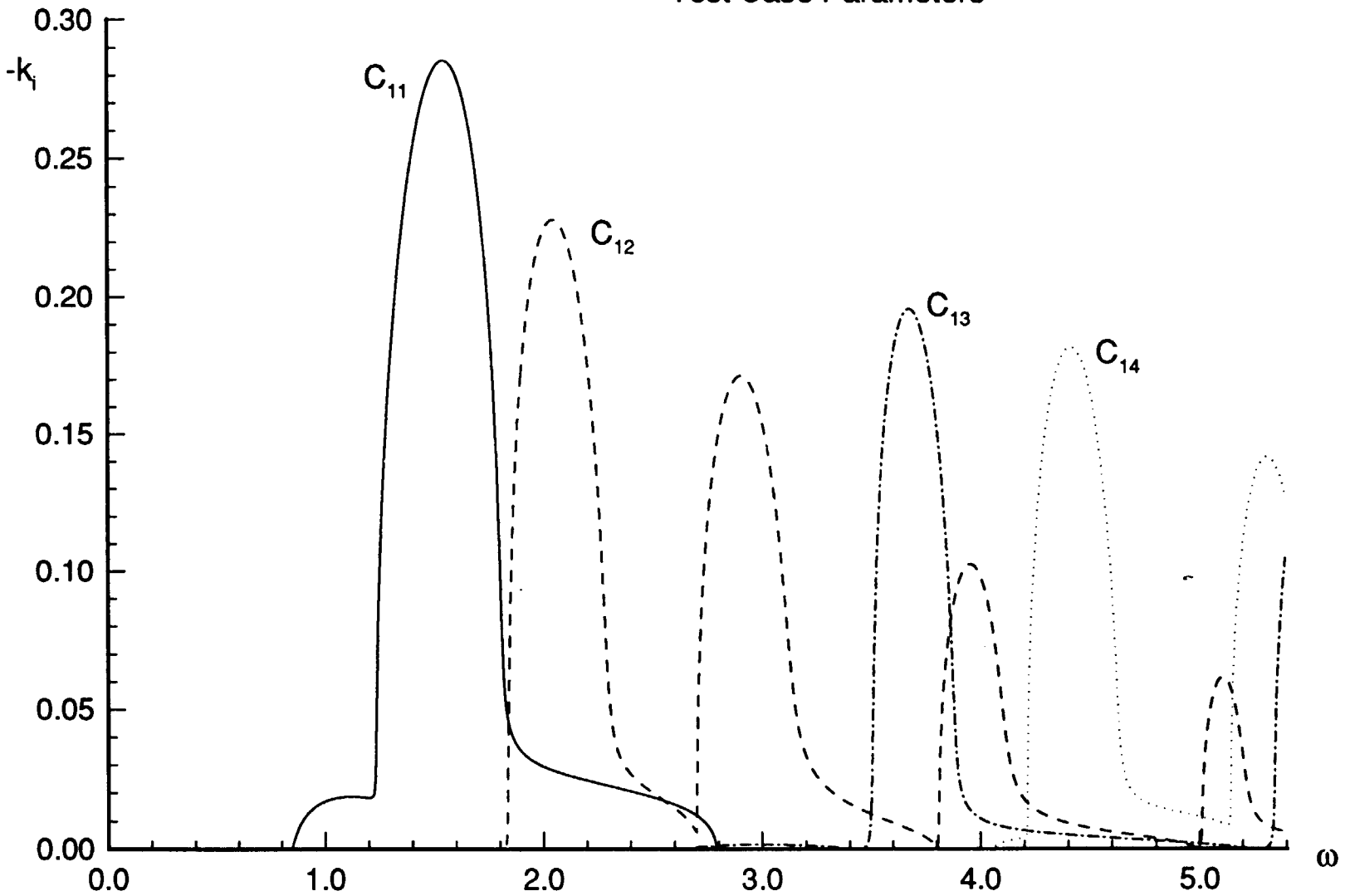

5d

Growth Rate vs. Frequency for the D_{11} Mode
($B = 2H$, $\beta = 2m\pi/B$, $m = 1$)

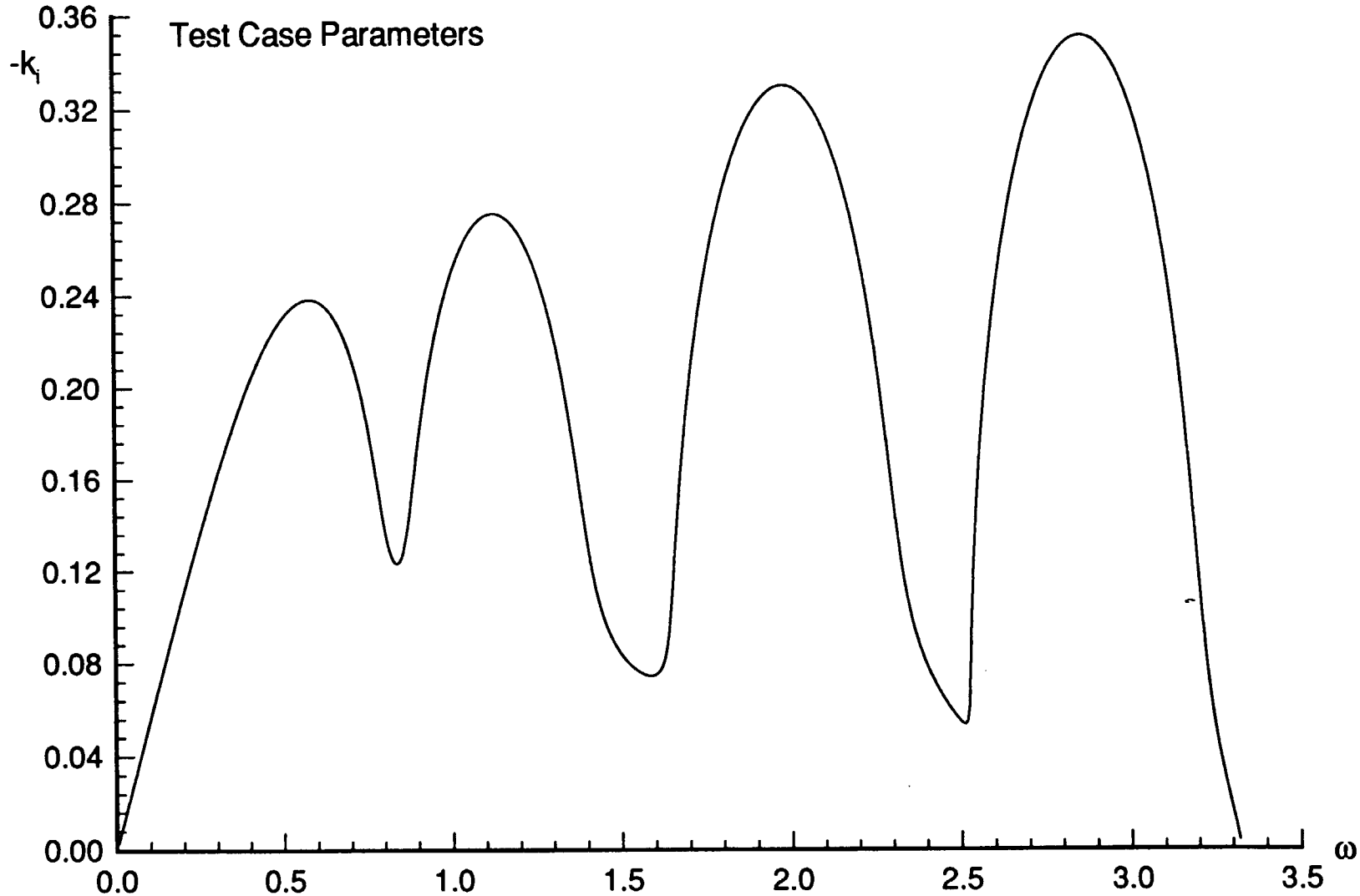

Contours of $|M_c(y)|_{max}$ for $\beta = 3\pi$

Test Case Parameters

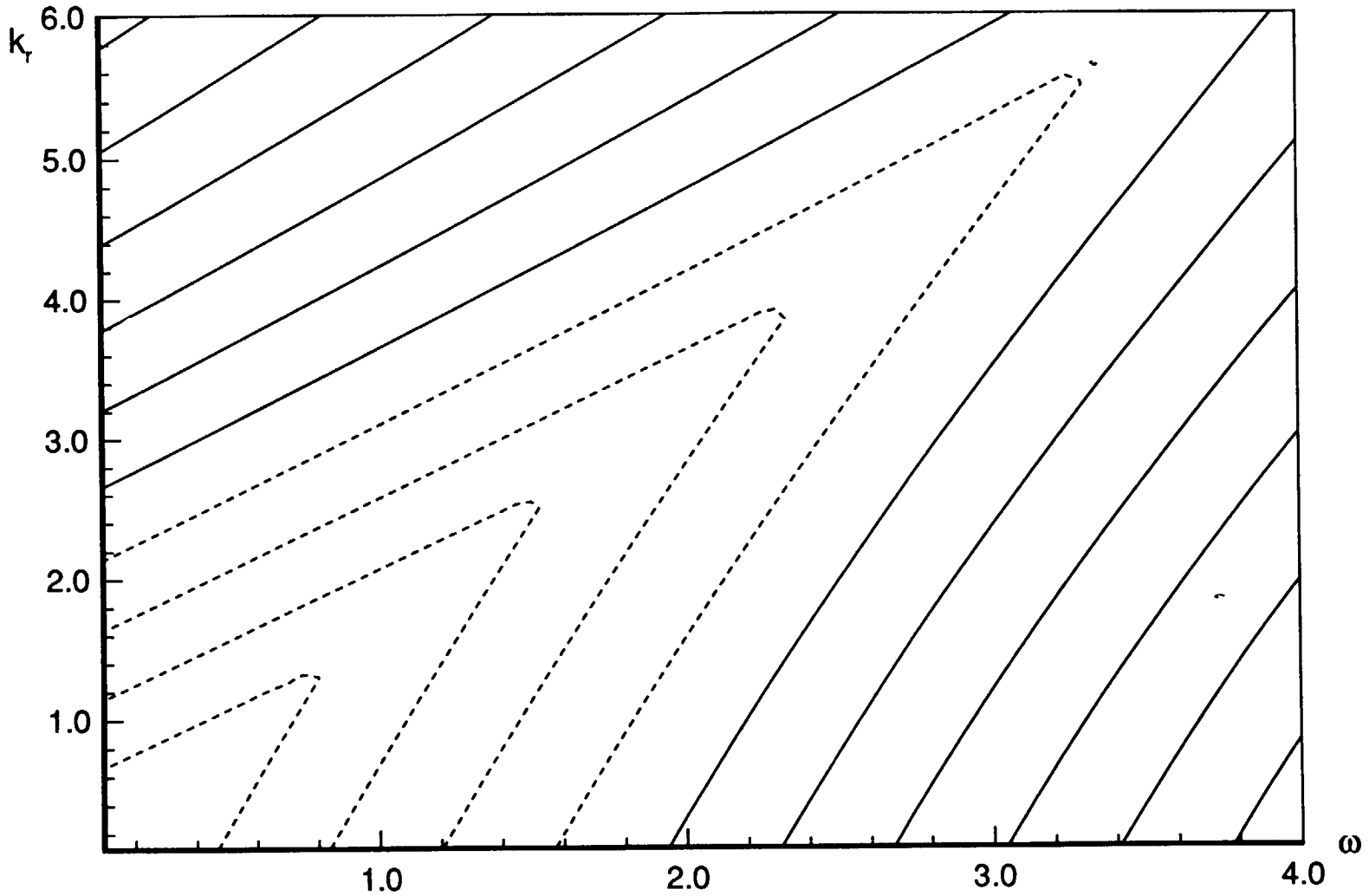

Streamwize Wavenumber vs. Frequency for All 3-D Modes
(B = 2H, β = 2mπ/B, m = 3)

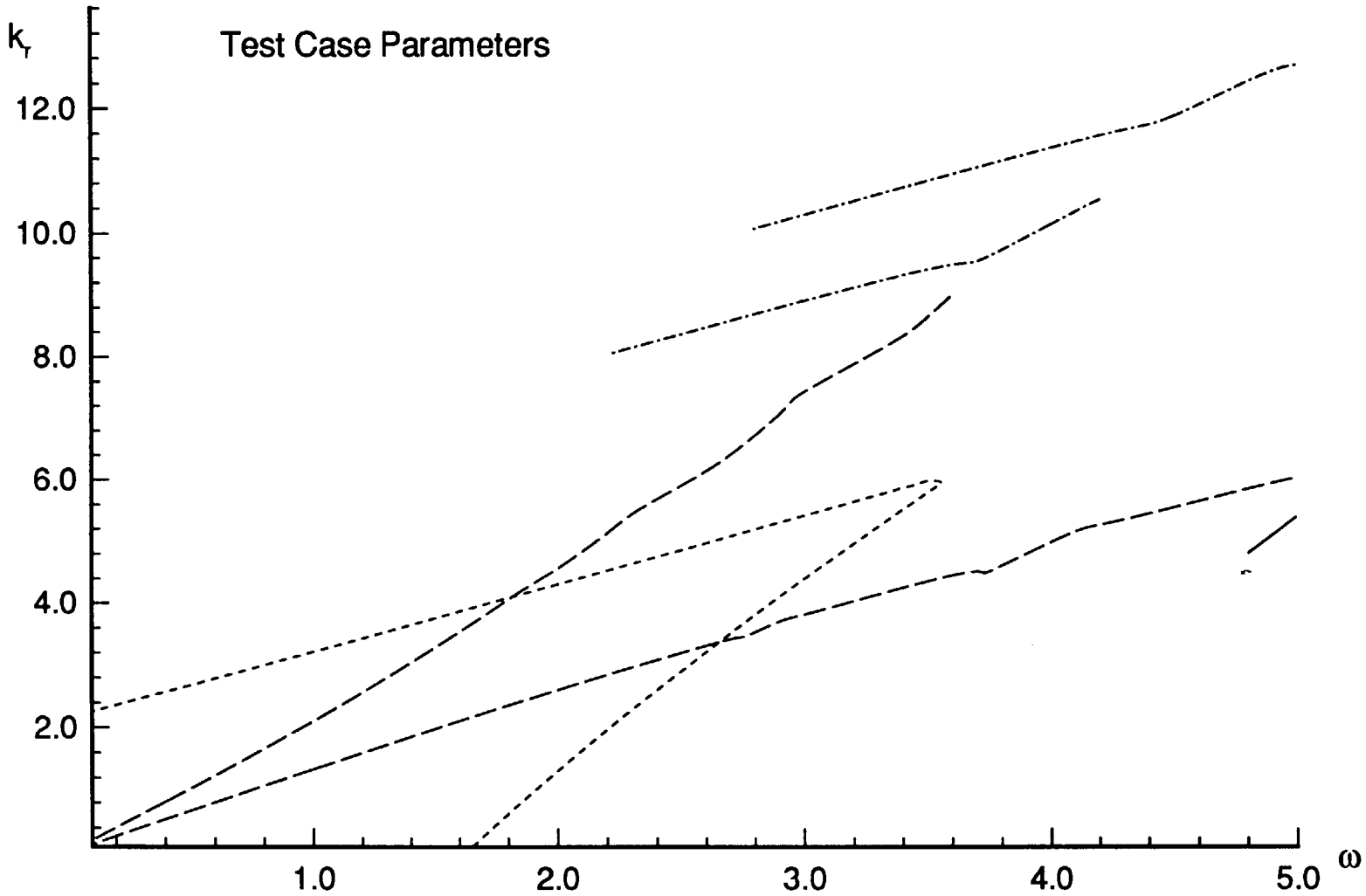

Phase Speed vs. Frequency for All 3-D Modes Based on the Boundary Layer Profiles

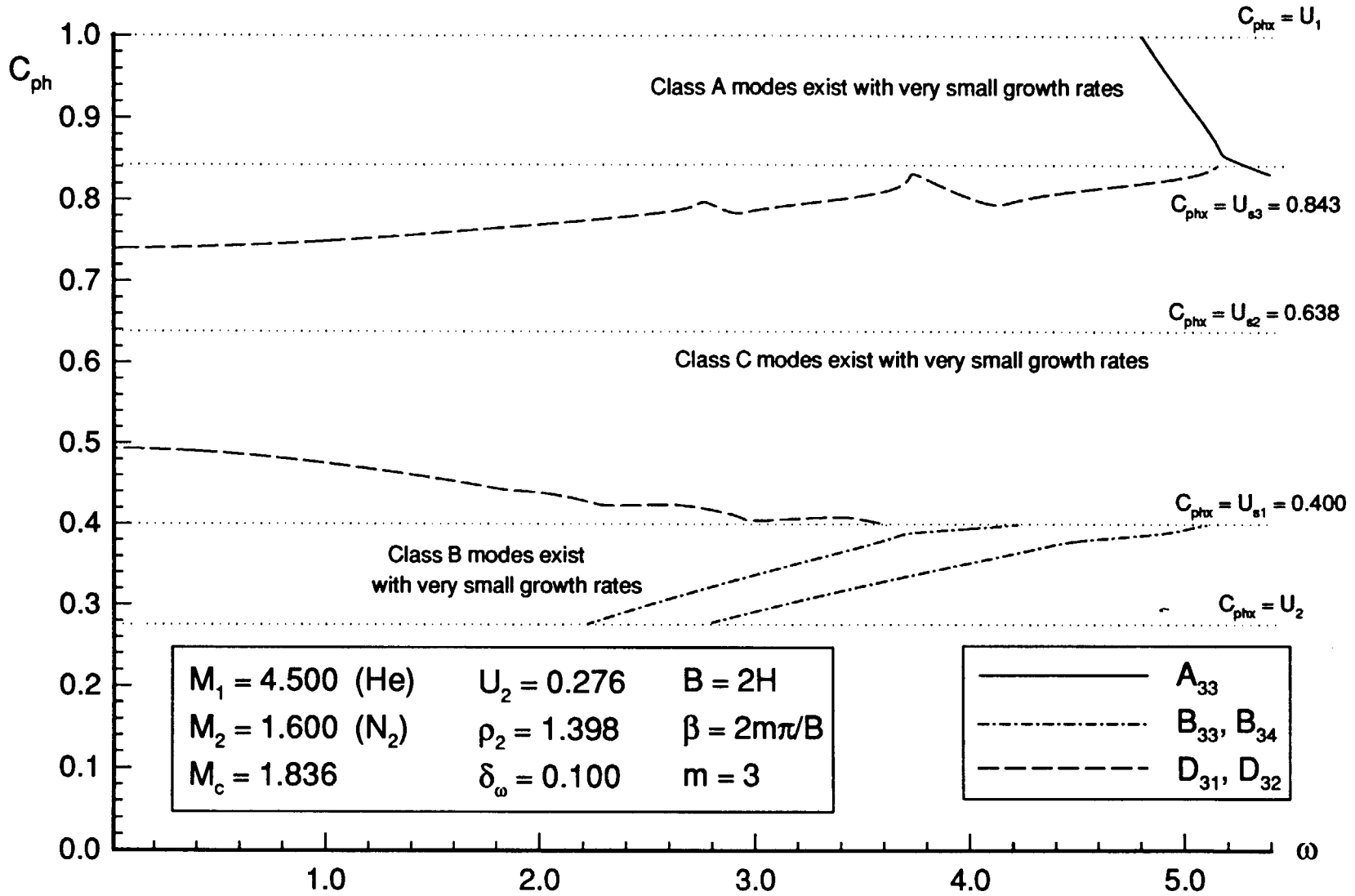

Growth Rate vs. Frequency for the Rest of the 3-D Mode

(B = 2H, β = 2mπ/B, m = 3)

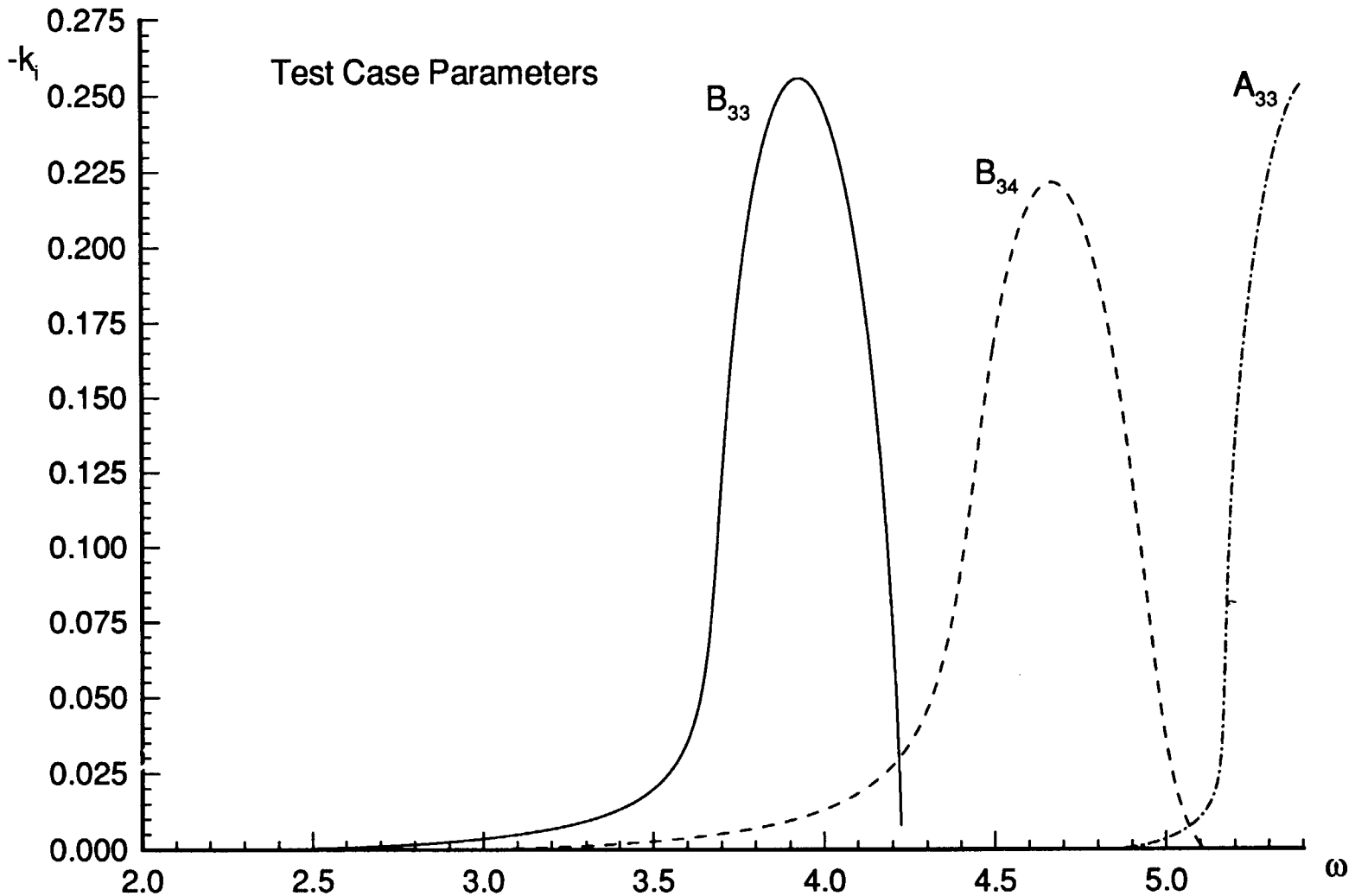

Growth Rate vs. Frequency for Class D Modes

(B = 2H, $\beta = 2m\pi/B$, m = 3)

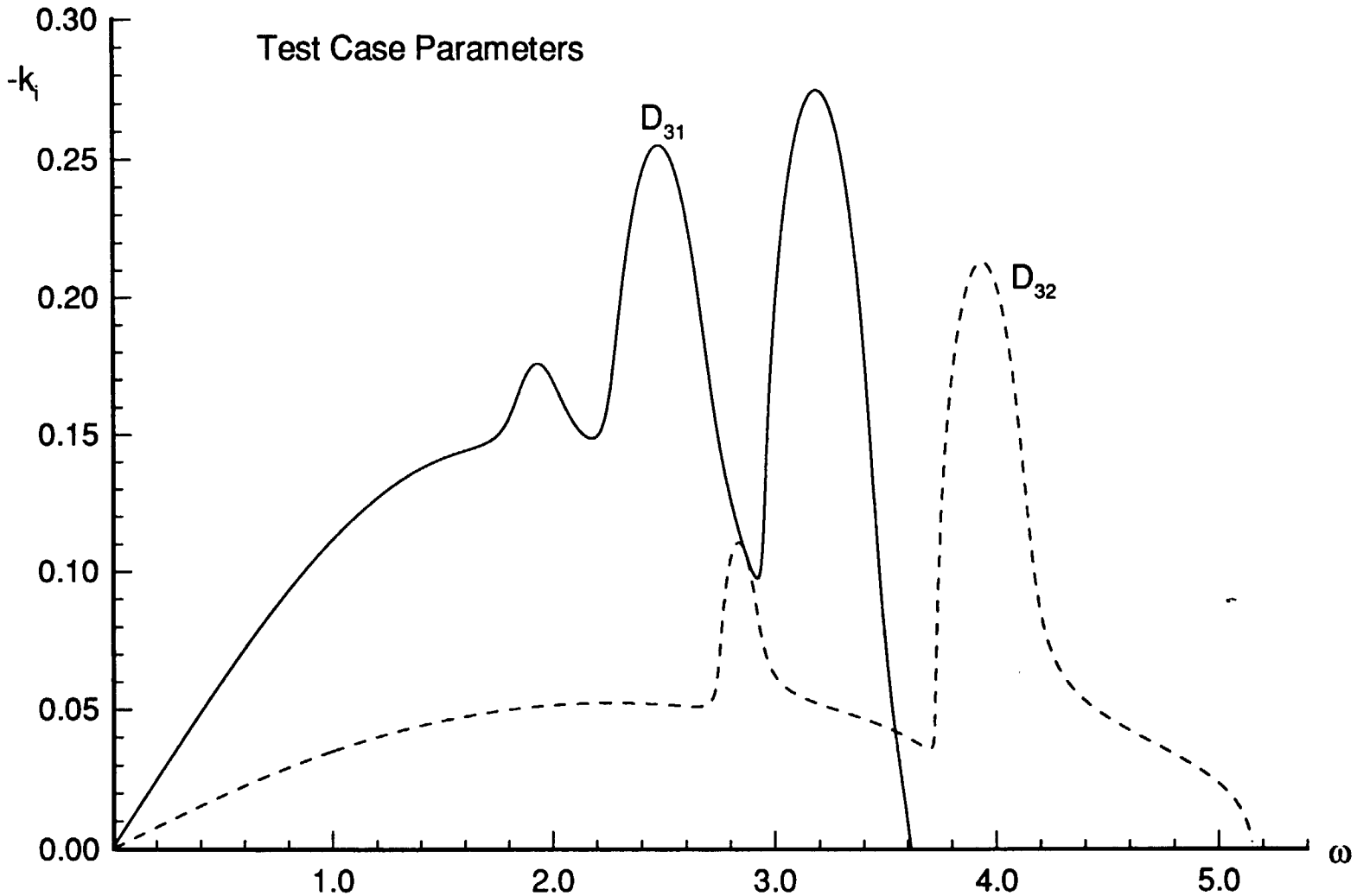

Streamwise Wavenumber vs. Frequency for All 3-D Modes

($B = 2H$, $\beta = 2m\pi/B$, $m = 1$)

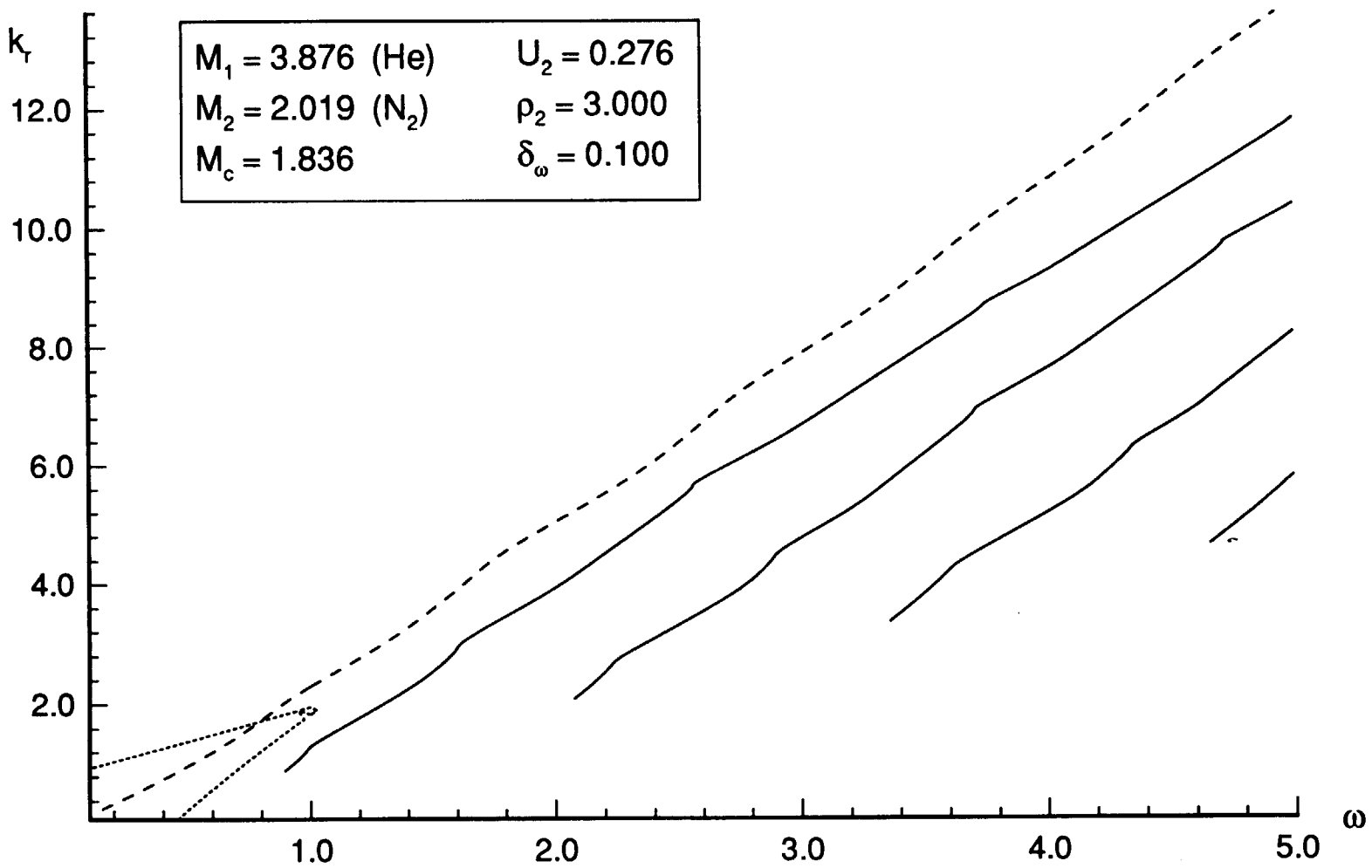

The triangular fine-dashed line is $|M_c(y)|_{max} = 1.0$

Phase Speed vs. Frequency for All 3-D Modes
Based on the Boundary Layer Profiles

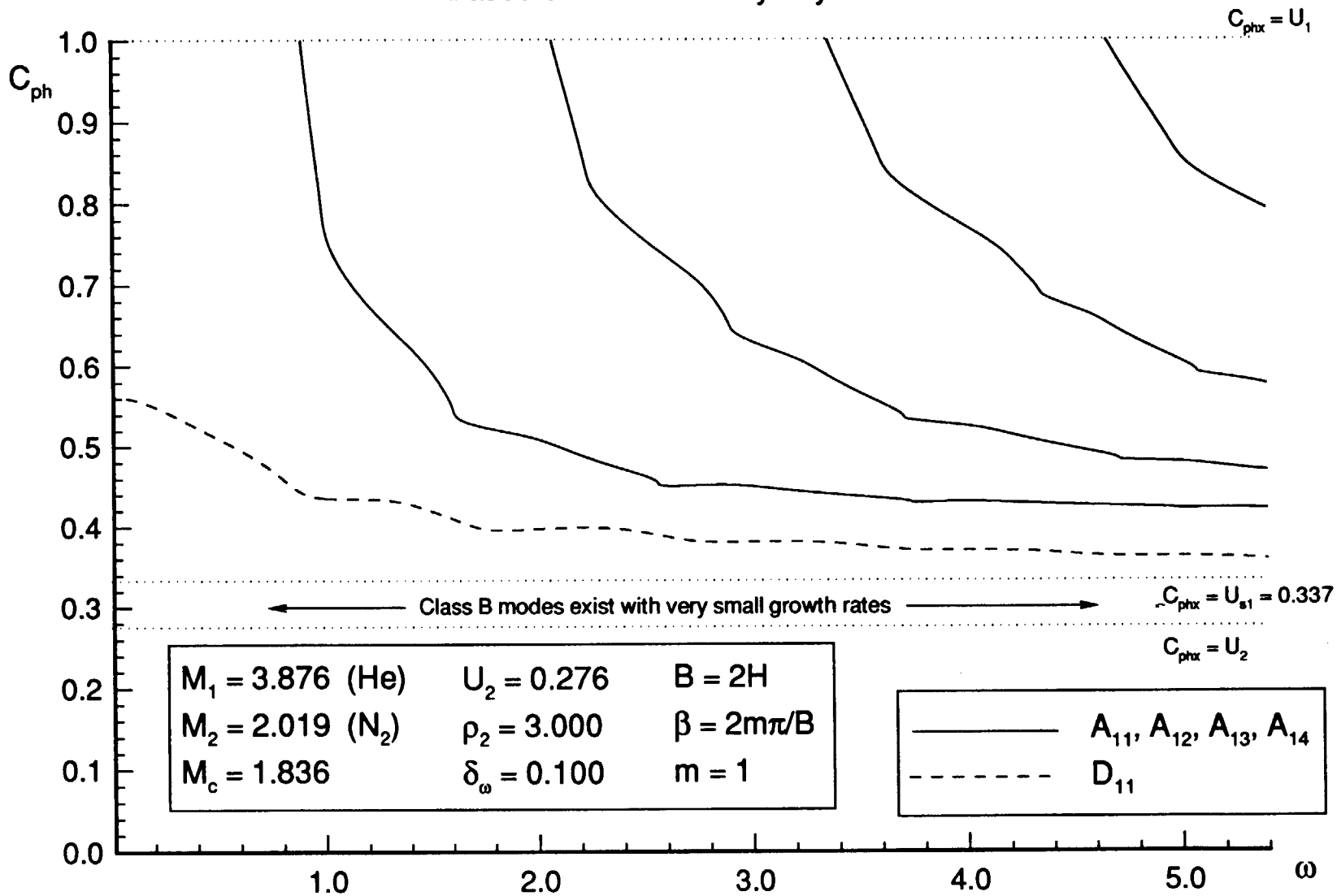

Growth Rate vs. Frequency for the Class A 3-D Modes

(B = 2H, β = 2mπ/B, m = 1)

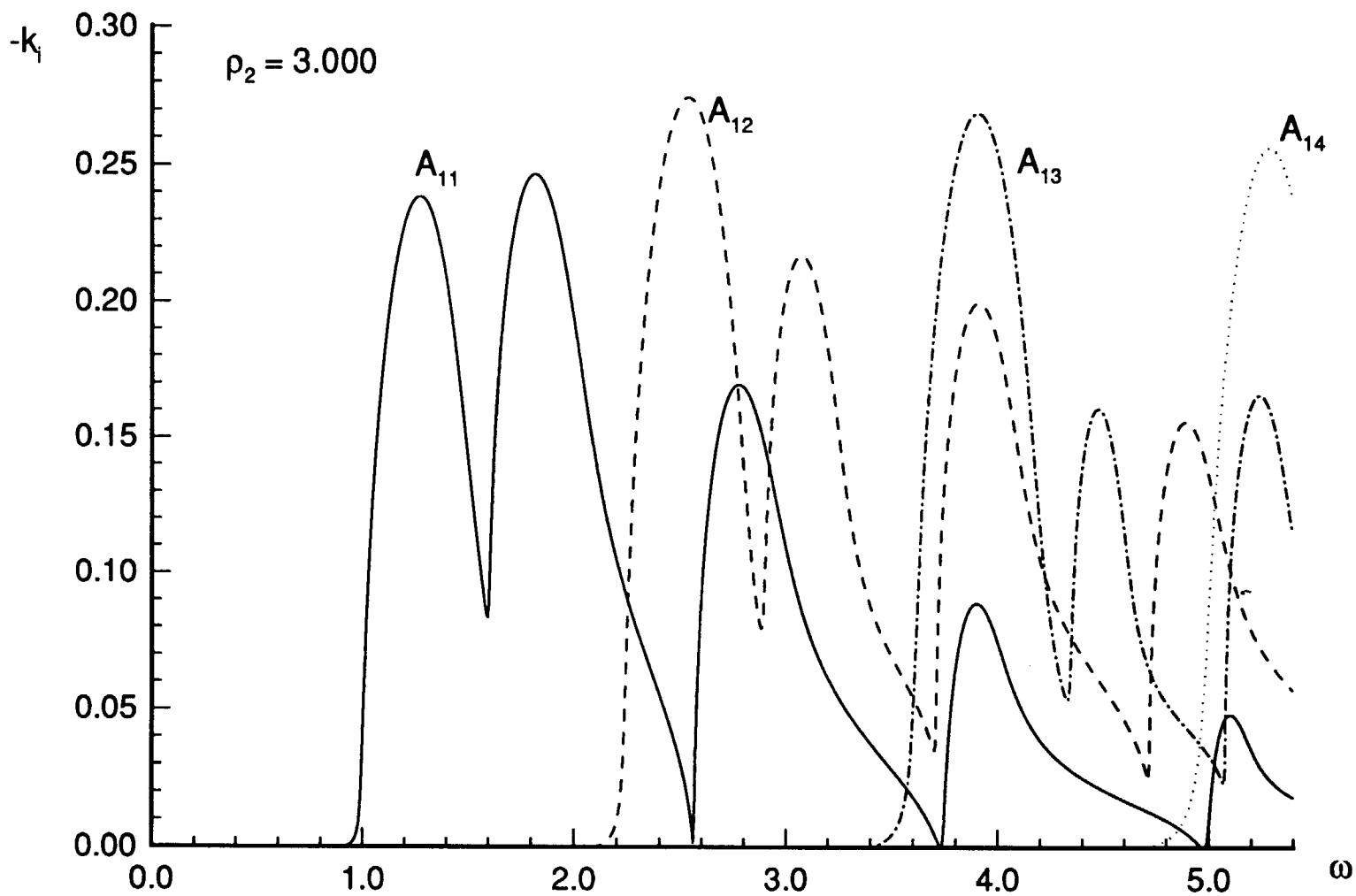

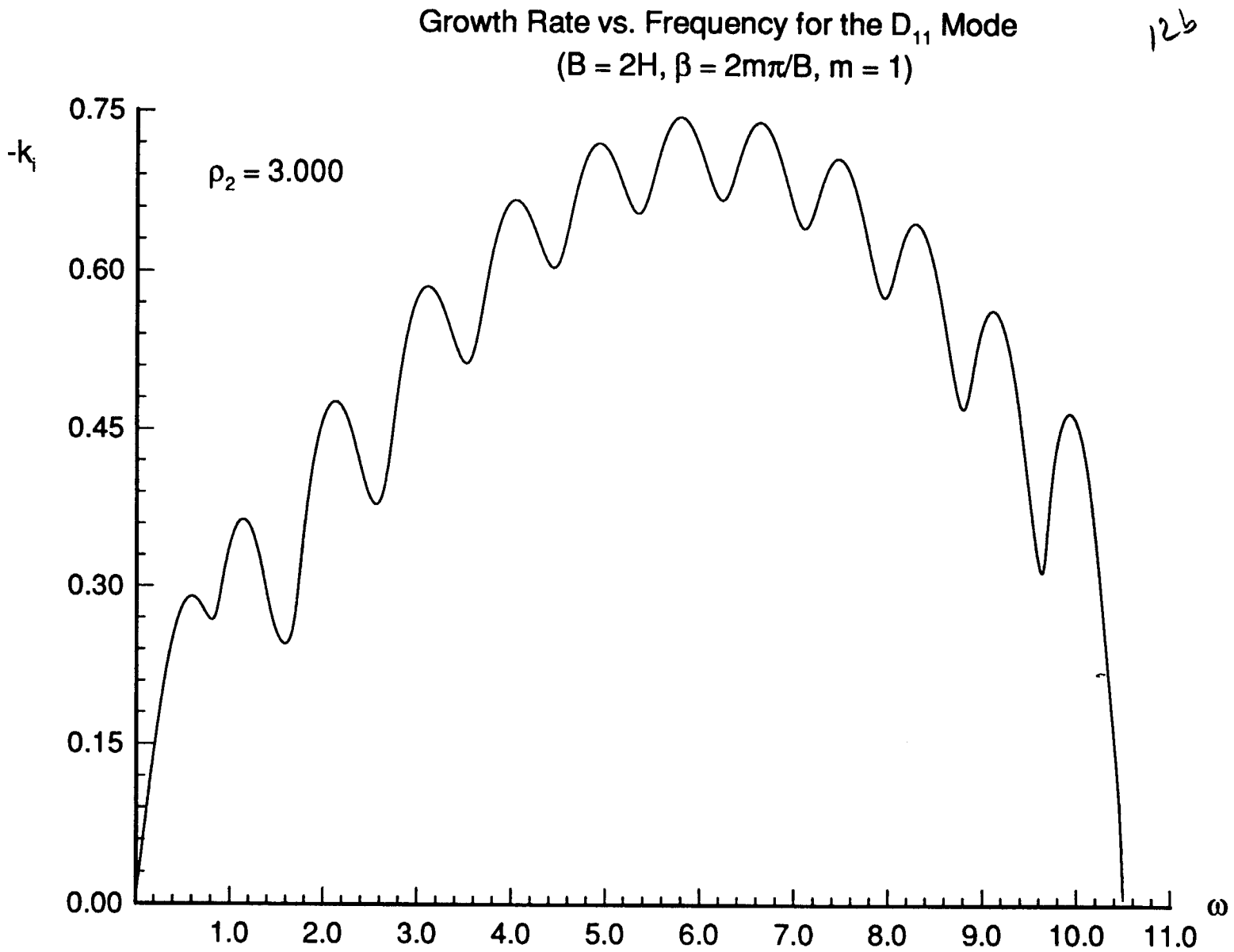
Growth Rate vs. Frequency for the D_{11} Mode
(B = 2H, β = 2mπ/B, m = 1)
$-k_i$
$\rho_2 = 3.000$
0.75
0.60
0.45
0.30
0.15
0.00
1.0
2.0
3.0
4.0
5.0
6.0
7.0
8.0
9.0
10.0
11.0
ω

Growth Rate vs. Frequency

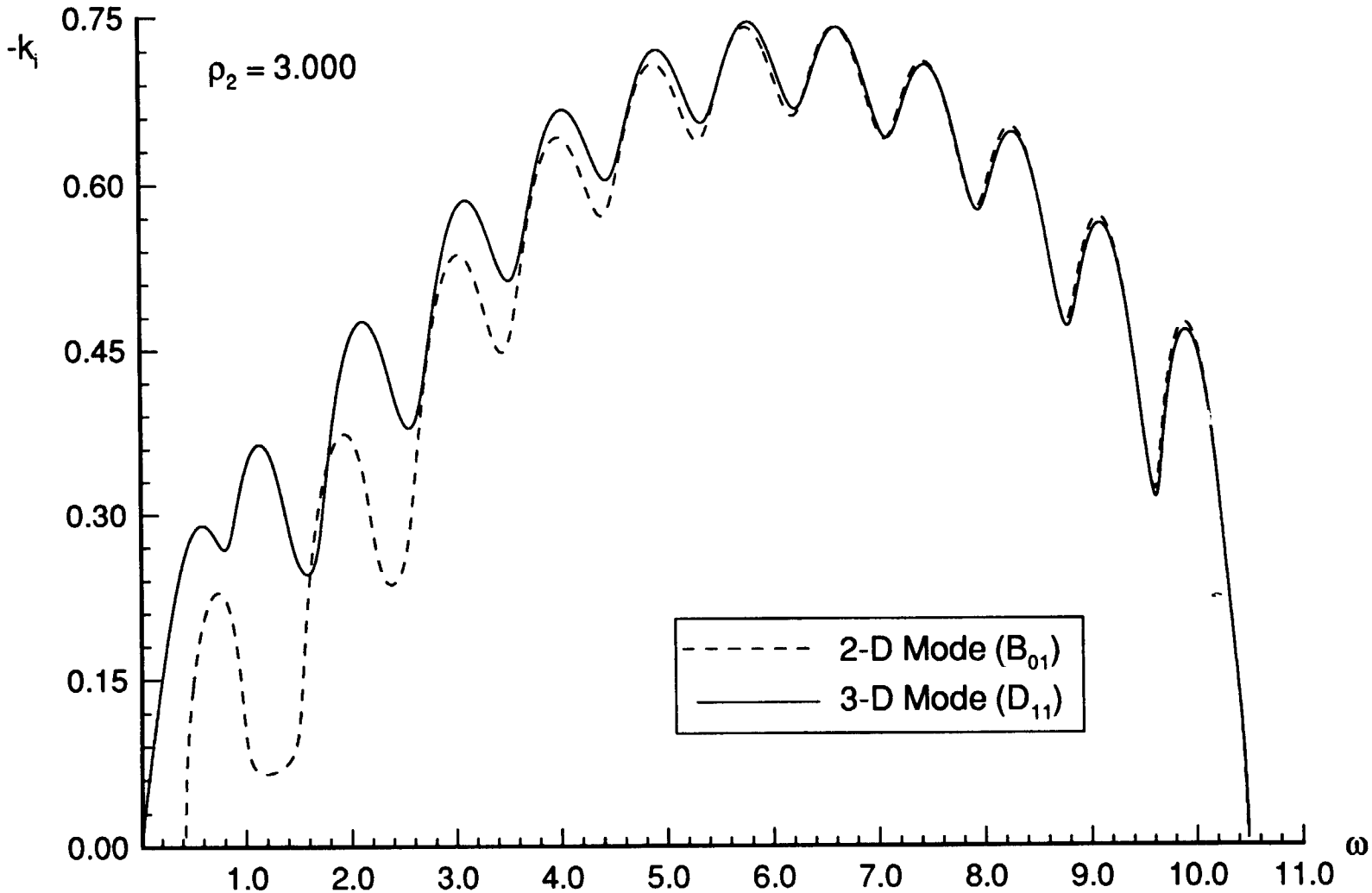

Wavenumber vs. Frequency for all the 3-D Modes
($B = 2H$, $\beta = 2m\pi/B$, $m = 3$)

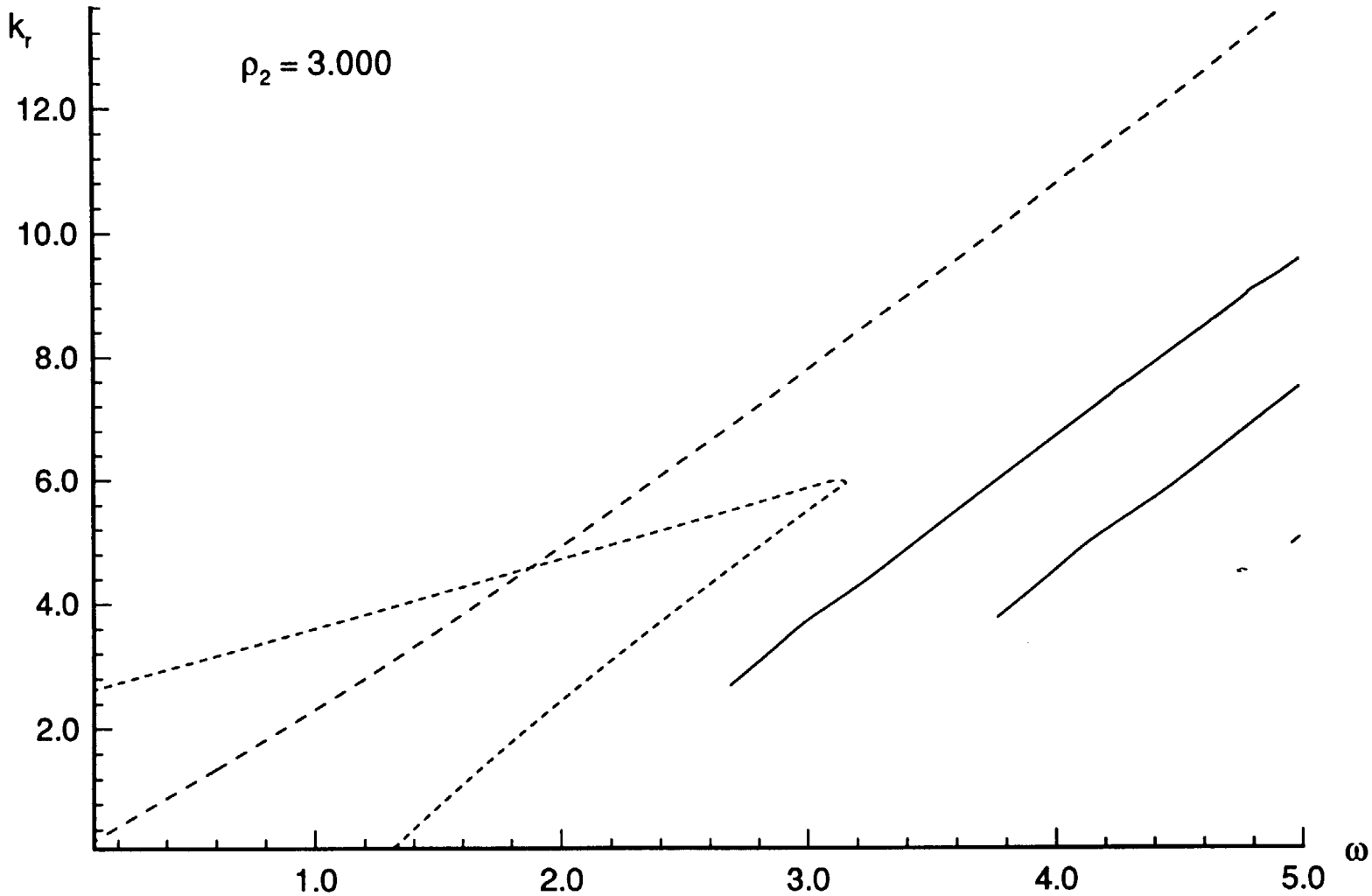

Phase Speed vs. Frequency of all the 3-D Modes

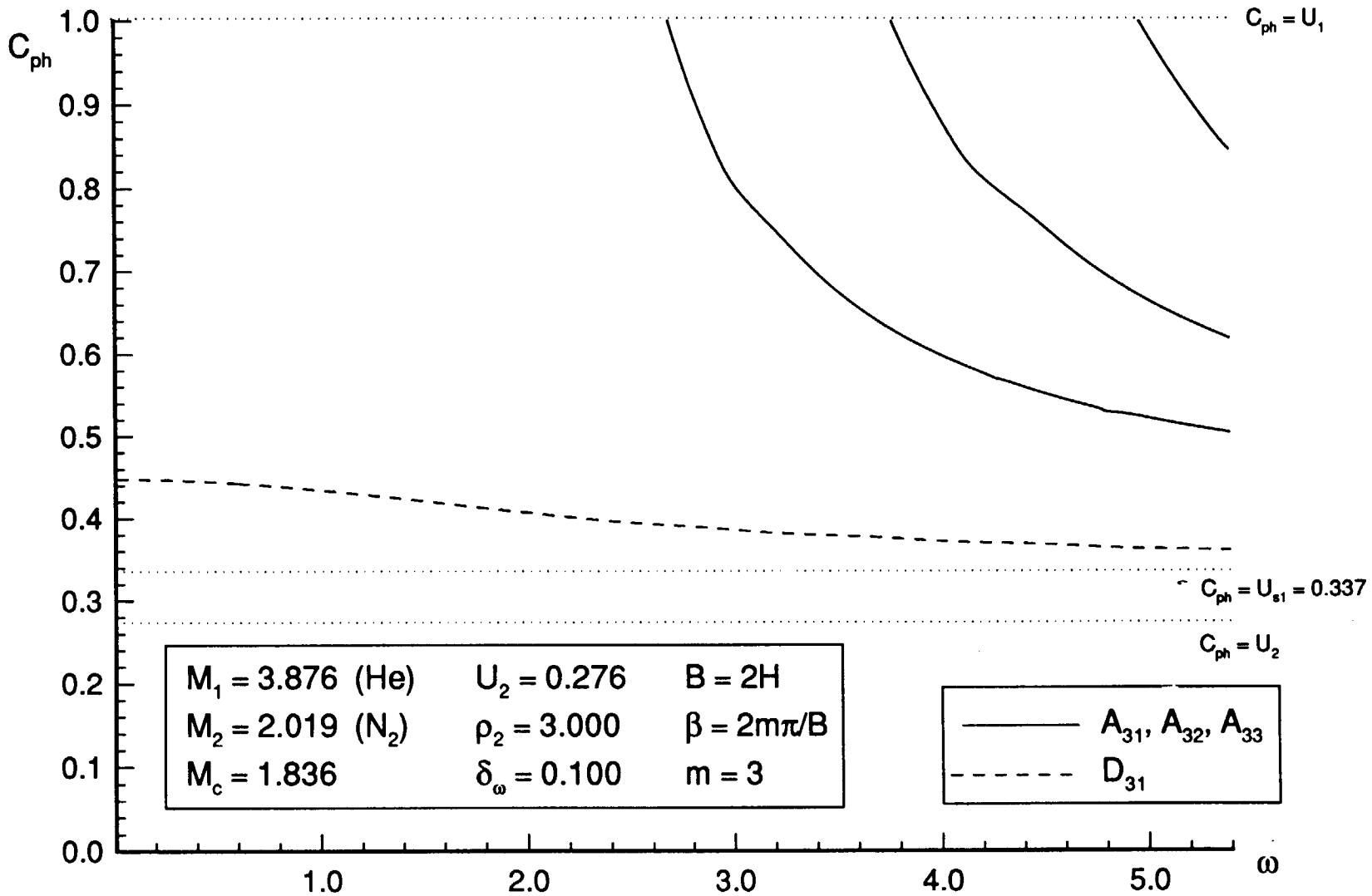

Growth Rate vs. Frequency for the Class A 3-D Modes

($B = 2H$, $\beta = 2m\pi/B$, $m = 3$)

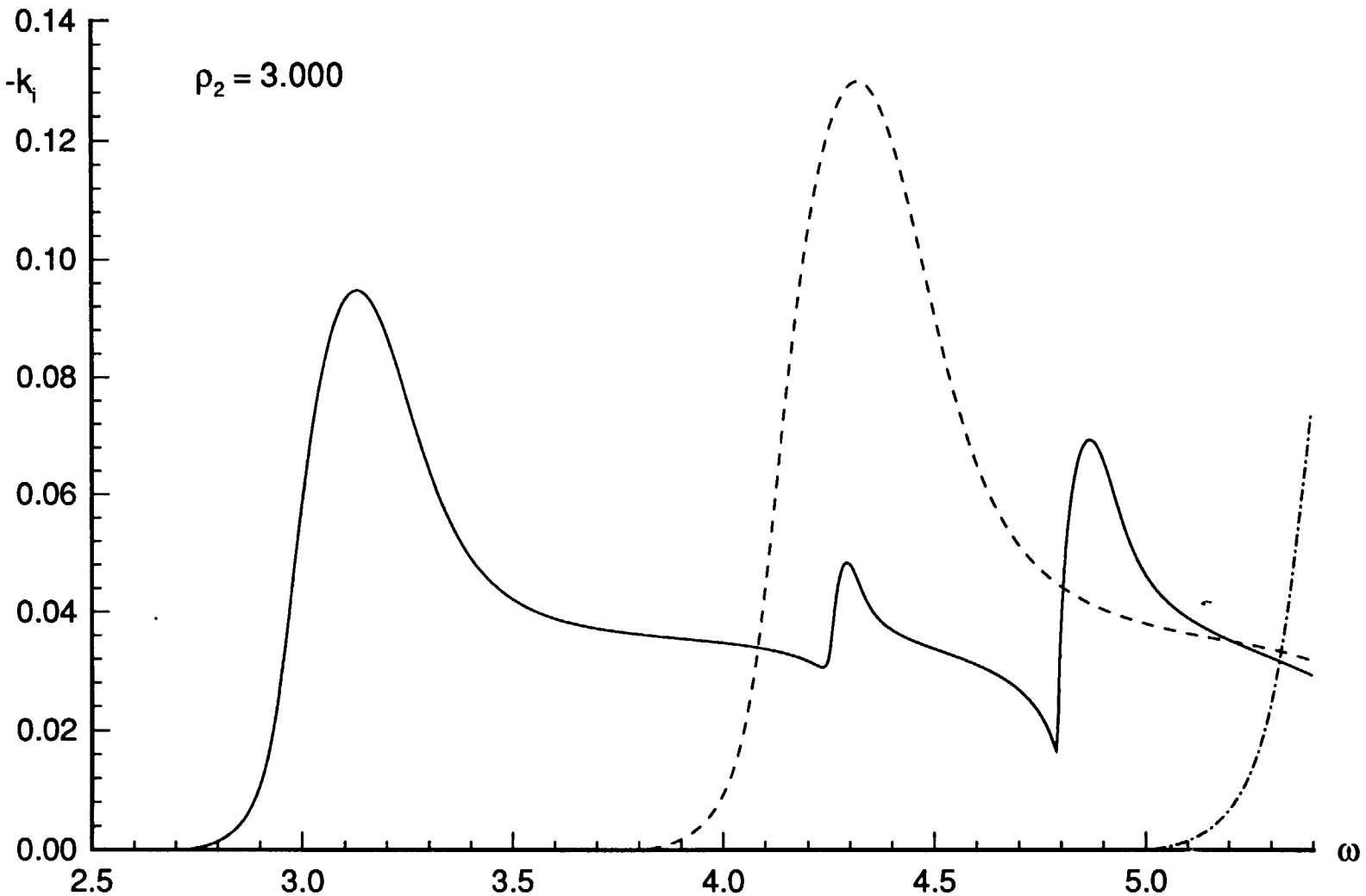

Growth Rate vs. Frequency for the D_{01} Mode

(B = 2H, $\beta = 2m\pi/B$, m = 3)

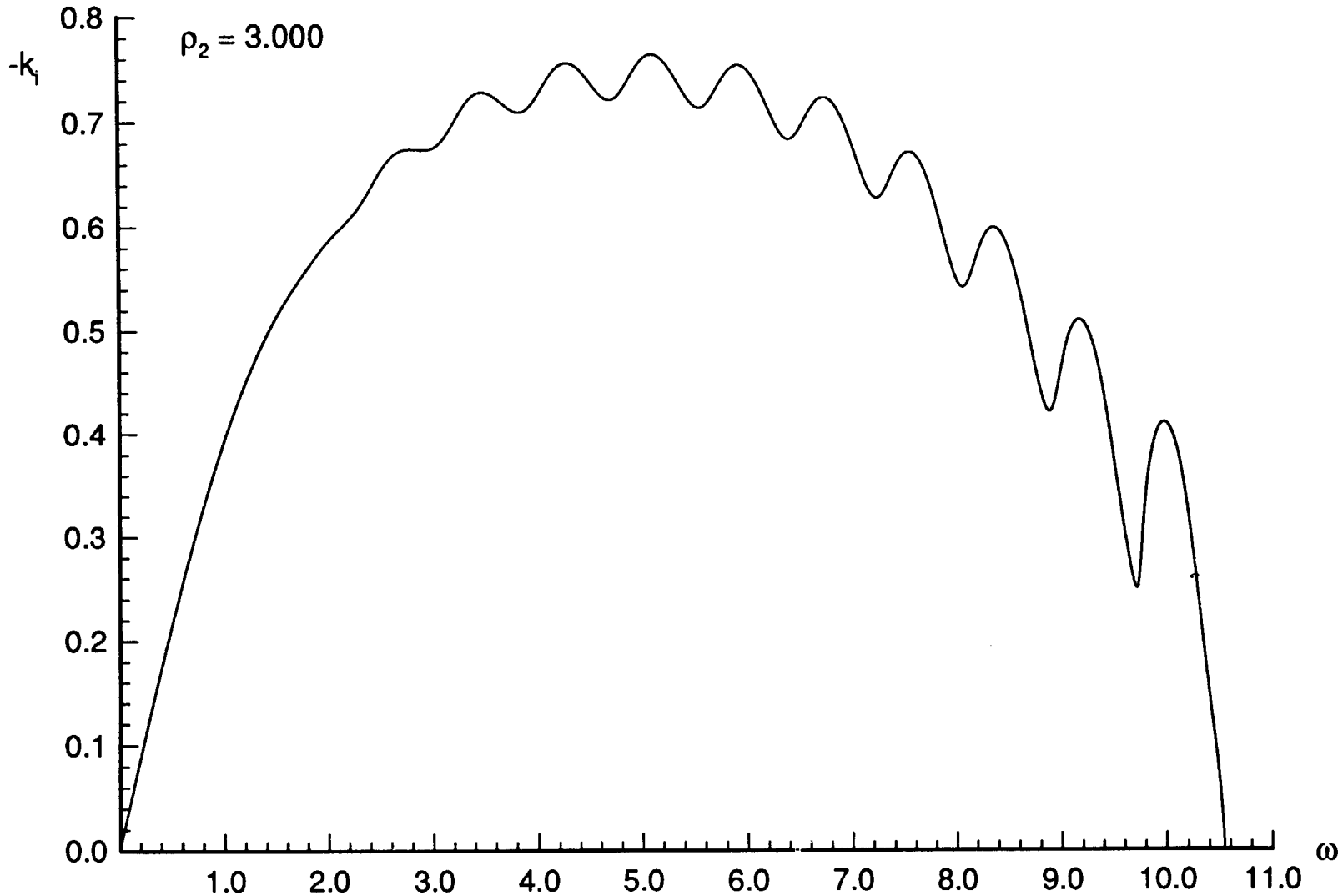

Growth Rate vs. Frequency
(B = 2H, β = 2mπ/B)